

## Development of direct numerical simulation database for supercritical carbon dioxide

S. Pandey, Prof. E. Laurien  
Institute of Nuclear Technology and Energy  
Systems (IKE), University of Stuttgart,  
70569, Stuttgart, Germany

Dr. X. Chu  
Institute of Aerospace Thermodynamics (ITLR),  
University of Stuttgart, 70569,  
Stuttgart, Germany



*Mr. Sandeep Pandey is currently working as a doctoral candidate at IKE, University of Stuttgart, Germany. He holds Master of Technology in Energy Studies from Indian Institute of Technology Delhi, India.*



*Dr. Eckart Laurien is Professor, Deputy Executive Director and Head of Thermo-Fluid Dynamics (TFD) group at Institute of Nuclear Technology and Energy Systems (IKE), University of Stuttgart, Germany.*



*Dr. Xu Chu is currently working as research associate at Institute of Aerospace Thermodynamics, University of Stuttgart, Germany. His area of expertise is supercritical fluids, porous media and turbulent flow.*

### ABSTRACT

Supercritical carbon dioxide (sCO<sub>2</sub>) has a wide spectrum of application in different fields such as working fluid in energy production and conversion industries. This spectrum covers both heating as well as cooling of the working fluid. Heat transfer and hydraulic characteristics are peculiar in the near-critical region due to the sharp variation of thermophysical properties in a narrow temperature range. Therefore, in this work, direct numerical simulations (DNSs) have been conducted with positive as well as negative heat flux to resemble the uniform heating and cooling, respectively. These DNSs were performed by utilizing the finite volume method. The diameter of the tube ranges between 2-10 mm corresponding to the hydraulic diameter of compact heat exchangers and it is assumed to be vertically oriented to avoid any thermal stratification. Through these DNSs, we have investigated forced convection (gravity neglected) and mixed convection (both upward and downward direction). These simulations were conducted at different inlet pressures, temperatures and heat flux. During heat rejection, stream-wise wall temperature distribution shows different trends for all three cases, which is primarily caused by the combined effect of fluid deceleration and buoyancy force. A sharp drop in wall temperature was observed in upward flow at the inlet and then it approximately remains constant, while wall temperature monotonically decreases in the downward flow and indicates the heat transfer deterioration. On the other hand, during heating vice versa of cooling was observed. We only focused on the deteriorated heat transfer cases in the heating. Along with the basic statistics, we used some advanced turbulence techniques to study the reasons for the dissimilar behavior of heat transfer. From these studies, it was found out that modulation in the near-wall turbulence leads to a different trend in heat transfer. This work not only limited to the investigation of heat transfer but with this work, we are delivering a comprehensive DNS database for benchmarking and calibration purpose.

*Keywords:* direct numerical simulation, supercritical carbon dioxide, heat transfer, database

## INTRODUCTION

Climate change is a major potential threat globally and it motivated researchers to increase the energy efficiency of existing energy-conversion techniques. In this regard, supercritical fluids are preservative working fluid to enhance the energy-conversion efficiency. The lower critical pressure and temperature of carbon dioxide ( $P_c=7.38$  MPa,  $T_c= 304.25$  K) as compared to water ( $P_c=22.06$  MPa,  $T_c= 674.09$  K) provide an opportunity to generate power in the reduced operating range [1,2]. The supercritical carbon dioxide (sCO<sub>2</sub>) finds its application in numerous areas, e.g., solar thermal, geothermal, nuclear, heat pumps [2]. However, sCO<sub>2</sub> suffers from peculiar heat transfer behavior in the near-critical region. Heat transfer deterioration was observed in the near-critical region for heating of sCO<sub>2</sub> in various experiments, in which the wall temperature increased significantly due to the poor heat transfer between the wall and bulk fluid [4]. This deteriorated heat transfer regime creates the problem of an accurate and reliable prediction of heat transfer arises in the near-critical region, for e.g. at 7.7 MPa, where almost all thermophysical properties change abruptly as shown in fig. 1. Along with experiments, computational fluid dynamics (CFD) studies are an important tool which provides insight information. Numerous attempts have been made in the past to model the heat transfer to sCO<sub>2</sub> by means of turbulence modeling [5-7]. He et al. [5] assessed low-Reynolds number turbulence models and found that models either over-predict or under-predict the heat transfer depending upon their damping function characteristics with respect to buoyancy and flow acceleration. Analogous observations were reported by Sharabi et al. [6]. Pucciarelli and Ambrosini [7] recently made an attempt to improve Reynolds-averaged Navier–Stokes (RANS) turbulence models. In this work, they incorporated an algebraic heat flux model as an auxiliary tool to calculate the turbulent Prandtl number distribution. This distribution was further used in the energy equation. Through this, buoyancy induced phenomena were captured up to an extent but it was not general for further application with certainty. Therefore, it can be concluded that CFD studies with turbulence models are not reliable at supercritical pressure. However, direct numerical simulation (DNS) is an attractive alternative to overcome this difficulty at low Reynolds numbers. Bae et al. [8] performed a DNS of heated pipe flow and elucidated the statistics of various turbulent quantities. Various flow conditions were simulated and they correspond to variations in the heat flux, tube diameter, gravity and flow direction. The authors observed heat transfer deterioration in upward flow and enhancement during the downward flow. Chu and Laurien [10] performed a DNS for a horizontally-oriented pipe, in which the gravity force affected the heat transfer in the transverse direction. They analyzed the heat transfer aspect and documented a secondary flow causing the flow stratification. Nemati et al. [10] also accomplished DNS and illustrated that reduction of the turbulent kinetic energy (TKE) leads to the heat transfer deterioration.

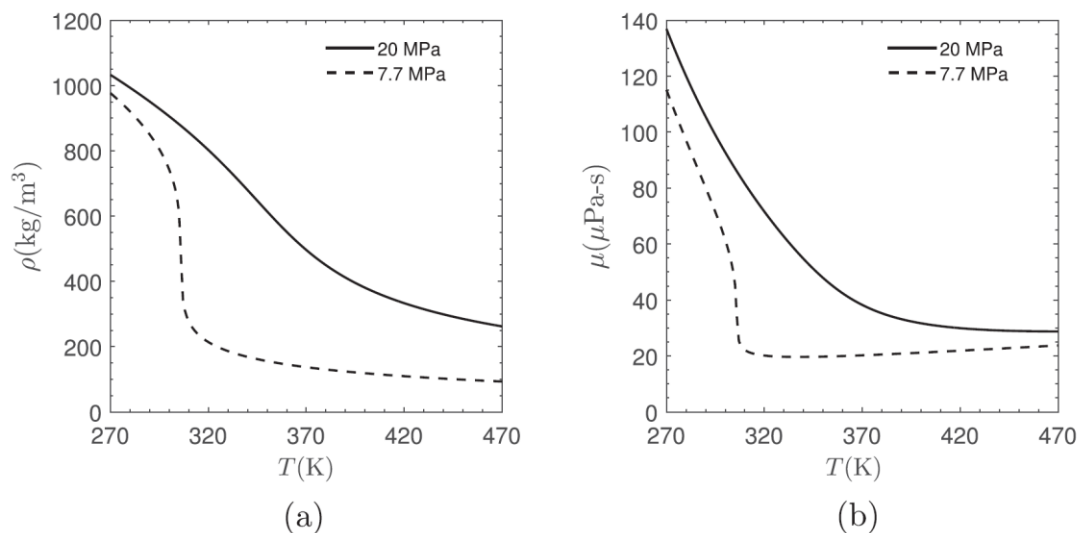


Figure 1: Variation of (a): Density, (b): Dynamic viscosity with temperature [3]

It is clear that turbulence models for RANS still have certain limitations in terms of accuracy and reliability due to Jensen inequality and the assumption of isotropic turbulence. Therefore, direct numerical simulation is an attractive way to analyze the flow. Therefore, in this work, we made an attempt to simulate over 45 cases. It includes both heating and cooling at different pressure, diameter, inlet temperature and pressure. The extreme cases which show peculiar behavior in terms of heat transfer and hydraulic resistance, we examined them further by different turbulence techniques. The objective of this study is twofold: firstly to understand the role of turbulence during deteriorated heat transfer. Secondly, we will create a DNS database, so that an accurate reference is available for the empirical fitting of correlations and models. In the past, DNS data for heating were used for turbulence model benchmarking [5, 7]. Also, DNS data for heating were used for semi-analytical models development by Pandey et al. [13]. Additionally, new innovative methods based upon machine learning algorithm requires reliable database to train the network for further prediction. Therefore, this study will further support the model development and benchmarking for supercritical carbon dioxide.

## METHODOLOGY

Throughout these DNSs, we rely on the low-Mach assumption, which is a valid assumption for sCO<sub>2</sub> under normal operating conditions. This assumption was also employed by Bae et al. [8], Chu et al. [9, 11] and Nematı et al. [10]. Following equations 1-3 show the conservation of mass, momentum, and energy for presented DNS.

$$\partial_t \rho + \nabla \cdot (\rho u) = 0 \quad (1)$$

$$\partial_t (\rho u) + \nabla \cdot (\rho u u) = -\nabla p + \nabla \cdot (2\mu S) \pm B_f \quad (2)$$

$$\partial_t (\rho h) + \nabla \cdot (\rho u h) = \nabla \cdot (2\kappa \nabla T) \quad (3)$$

In equations 1-3,  $\rho$  denotes the fluid density,  $u$  is the velocity vector,  $p$  is the pressure,  $\mu$  represents the dynamic viscosity,  $h$  is the specific enthalpy,  $\kappa$  is the thermal conductivity and  $T$  denotes the temperature. The  $B_f$  is the body force due to gravity and its value is  $[0, 0, \rho g]^T$  and  $S$  represents the strain tensor. The thermophysical were implemented by a piecewise spline functions. These properties were derived from NIST REFPROP [3] and error-bound of the derived spline function and the NIST database was within  $\pm 1\%$  for all thermophysical properties. Equations 1 to 3 were solved by finite volume method and such discretization schemes were used so that overall code has second-order accuracy in both space and time.

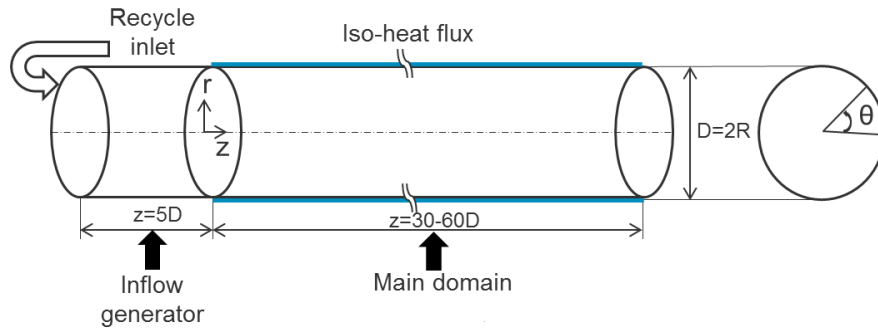


**Figure 2: Computational domain for the DNS**

The simulation domain consists of a tube of 2-10 mm diameter with a total length of 35-65 diameters as depicted in Fig. 2. The tube is divided into two parts: the inflow generator and the main domain. The inflow generator has a length of  $5D$ . The objective of this section is to provide a fully developed turbulent flow to the main domain at every time step. The main domain is distinguished from the inflow generator by a positive or negative uniform heat flux for the remaining length. In the main domain, the no-slip boundary condition is imposed at the wall while a convective outflow boundary condition is implemented

for the velocity and other variables at the outlet. The distinction between upward and downward flow is made by changing the direction of gravity in the momentum equation while the distinction between forced and mixed convection is made by omitting or including the gravity term in the momentum equation. This numerical procedure has been validated with the experiments as well as with the other DNS (refer [9, 12]).

## SIMULATION PARAMETERS

During this study, over 45 cases were simulated by means of DNS. This includes heating as well as cooling in the vertical orientation of tube. Table-1 and 2 give an overview of the DNS parameters. For heating, we conducted DNS only for upward flow, where the heat transfer peculiarity has been reported earlier. These were performed with 8 MPa and 8.8 MPa as the inlet pressure ( $P_0$ ), 288 K and 301 K as the inlet temperature ( $T_0$ ) with 3 different diameters of the pipe. Three different heat fluxes were chosen to depict the low, mid and high heat flux for a given mass flux. While during the heat rejection, all three possibilities (upward, downward and forced i.e. with zero gravity) were simulated for 2 mm diameter pipe. The database generated with DNS includes 47 cases in total. One case takes approximately 12000 core-hours on the Hazel Hen machine. It means that a total of about 550,000 core-hours are necessary to complete all the cases in the database. Each case is under one experimental condition.

**Table-1: Simulation parameters for heating cases; Denoted as “Sr. No.- Flow Direction (Diameter, Pressure, Temperature, Heat Flux)”**

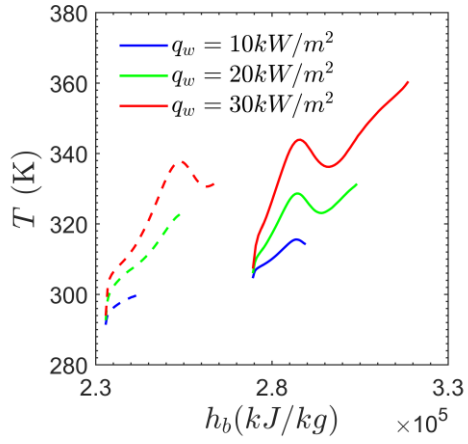
| $Re_0= 5400$   $L_t= 60D$   $T_0 = 288.15$ and $301.15$ K   $P_0= 8$ and $8.8$ MPa   $G = 30\sim 230$ kg/m <sup>2</sup> s |                     |                     |                    |                     |                     |
|---|---------------------|---------------------|--------------------|---------------------|---------------------|
| 1-U(2,8,301,10)   | 2-U(2,8,301,20)     | 3-U(2,8,301,30)     | 4-U(2,8,288,10)    | 5-U(2,8,288,20)     | 6-U(2,8,288,30)     |
| 7-U(2,8,8,301,10)   | 8-U(2,8,8,301,20)   | 9-U(2,8,8,301,30)   | 10-U(2,8,8,288,10) | 11-U(2,8,8,288,20)  | 12-U(2,8,8,288,30)  |
| 13-U(5,8,301,5)   | 14-U(5,8,301,10)    | 15-U(5,8,301,20)    | 16-U(5,8,288,5)    | 17-U(5,8,288,10)    | 18-U(5,8,288,20)    |
| 19-U(5,8,8,301,5)   | 20-U(5,8,8,301,10)  | 21-U(5,8,8,301,20)  | 22-U(5,8,8,288,5)  | 23-U(5,8,8,288,10)  | 24-U(5,8,8,288,20)  |
| 25-U(10,8,301,5)  | 26-U(10,8,301,10)   | 27-U(10,8,301,20)   | 28-U(10,8,288,5)   | 29-U(10,8,288,10)   | 30-U(10,8,288,20)   |
| 31-U(10,8,8,301,5)  | 32-U(10,8,8,301,10) | 33-U(10,8,8,301,20) | 34-U(10,8,8,288,5) | 35-U(10,8,8,288,10) | 36-U(10,8,8,288,20) |

**Table-2: Simulation parameters for cooling cases; Denoted as “Sr. No.- Flow Direction (Diameter, Pressure, Temperature, Heat Flux)”**

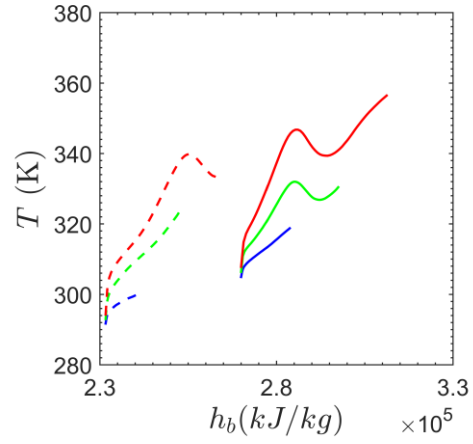
| $Re_0= 5400$   $L_t= 30D$   $T_0 = 342.05$ K   $P_0= 8$ and $8.8$ MPa   $G = 30\sim 230$ kg/m <sup>2</sup> s |                     |                     |                     |                     |                   |
|--|---------------------|---------------------|---------------------|---------------------|-------------------|
| 37-U(2,8,342,-30)  | 38-D(2,8,342,-30)   | 39-F(2,8,342,-30)   | 40-U(2,8,342,-60)   | 41-D(2,8,342,-60)   | 42-F(2,8,342,-60) |
| 43-U(2,8,8,342,-30)  | 44-D(2,8,8,342,-30) | 45-F(2,8,8,342,-30) | 46-U(2,8,8,342,-60) | 47-D(2,8,8,342,-60) |                   |

The cylindrical pipe is filled with the structured hexahedral mesh. Typically, DNS requires a huge amount of computational resource which resolves all the small-scale motions. Therefore, the grid resolution is reduced to 70×120×1500 for the main domain from the past work [9, 11, 13]. Nevertheless, this resolution is comparable to the classical work of Bae et al. [8]. From the grid independence study, we found that mean statistics (wall temperature and wall shear stress) have a negligible effect when compared to a very fine mesh (8 time finer mesh).

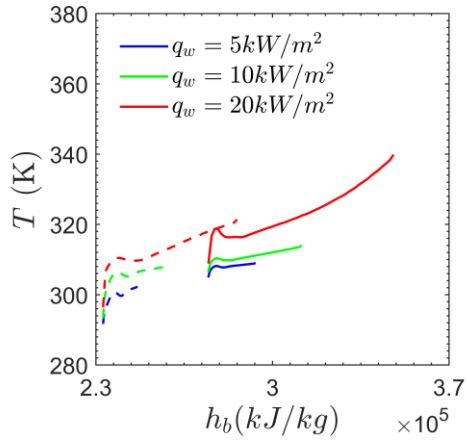
## RESULTS AND DISCUSSION



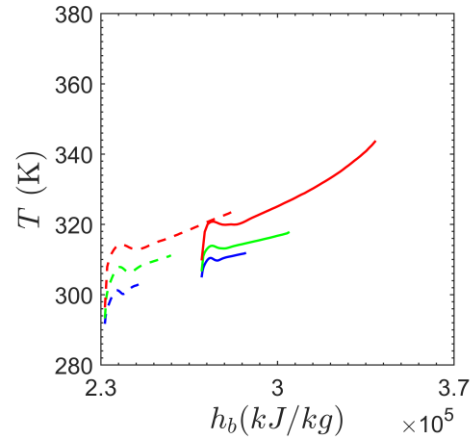
(a)



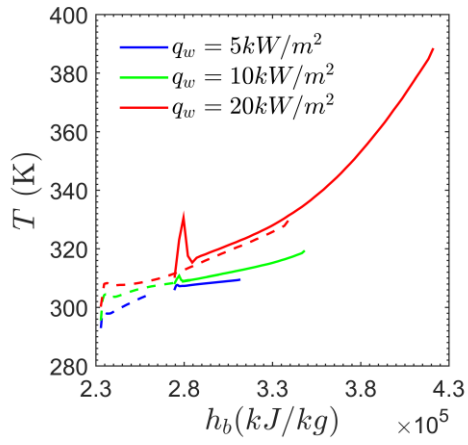
(b)



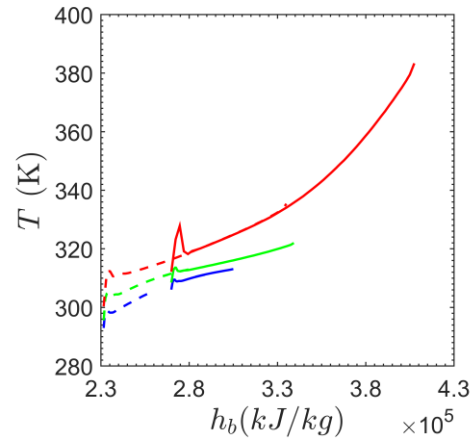
(c)



(d)



(e)



(f)

Figure 3: Variation of wall temperature; (a, b):  $D=2\text{mm}$ , (c, d):  $D=5\text{mm}$ , and (e, f):  $D=10\text{mm}$ ; first column= 8 MPa and second column 8.8 MPa; Dashed lines:  $T_0=288\text{K}$ , solid lines:  $T_0=301\text{K}$  (Case 1-36)

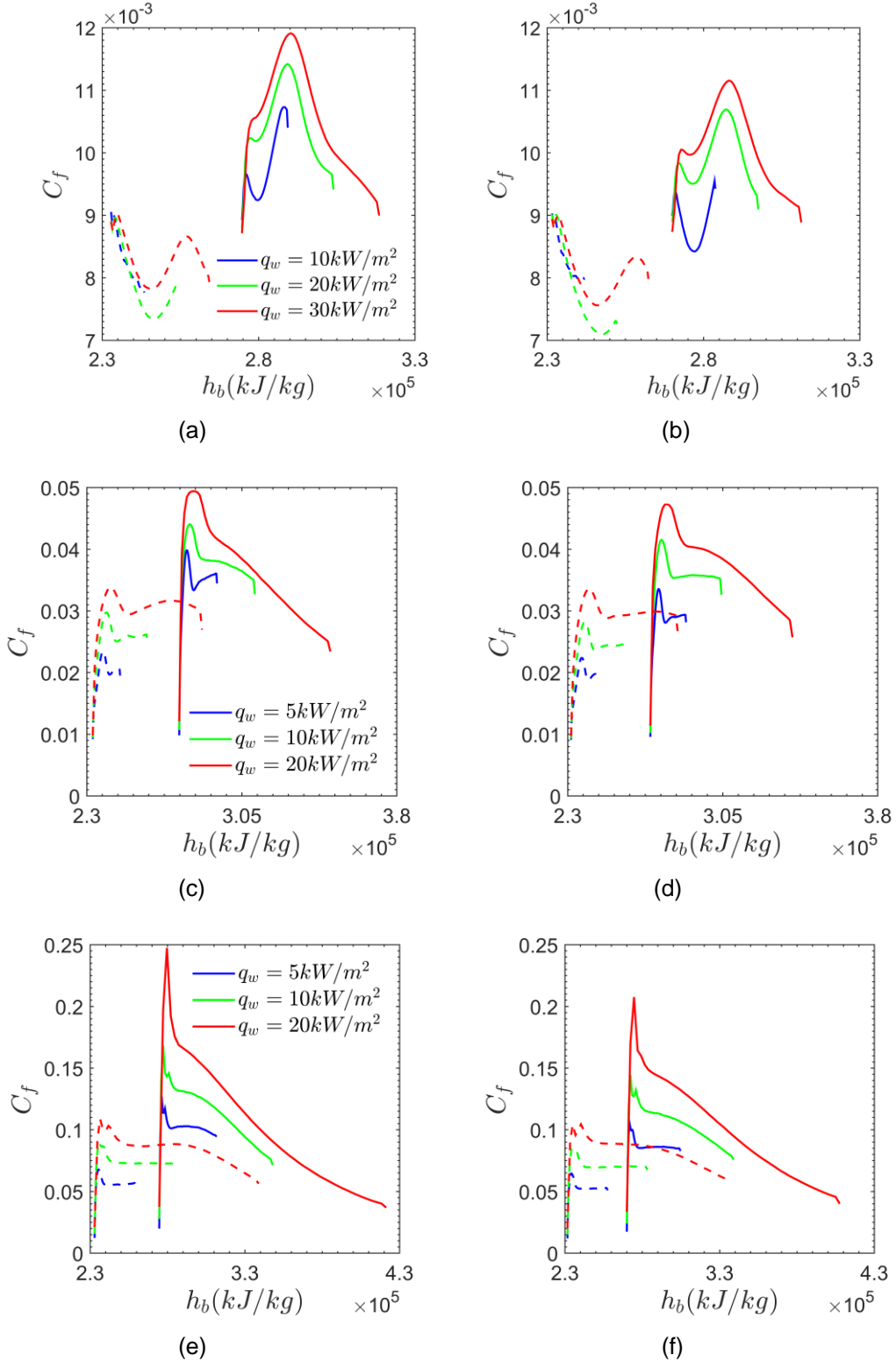
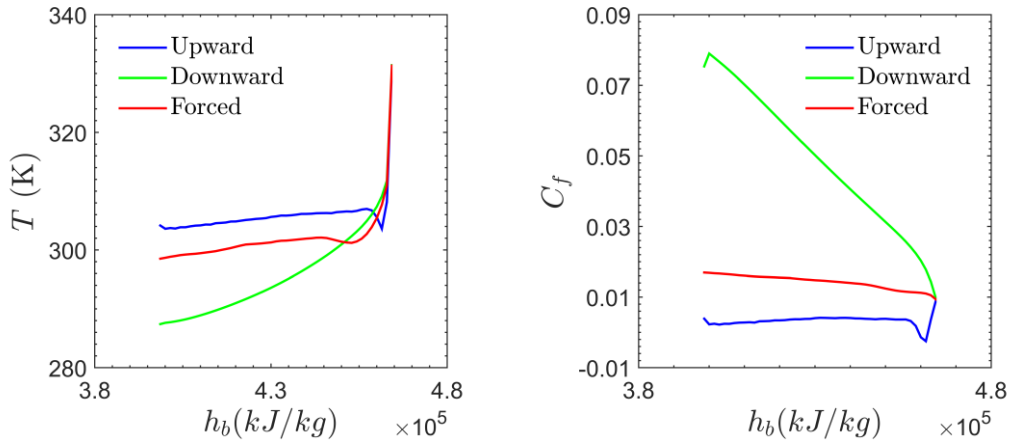


Figure 4: Variation of skin friction coefficient; (a, b):  $D= 2\text{ mm}$ , (c, d):  $D= 5 \text{ mm}$ , and (e, f):  $D= 10 \text{ mm}$ ; first column=  $8 \text{ MPa}$  and second column  $8.8 \text{ MPa}$ ; Dashed lines:  $T_w=288 \text{ K}$ , solid lines:  $T_w=301 \text{ K}$  (Case 1-36)

In this section, few important results from the DNSs are reported. Figure 3 and 4 show the variation of wall temperature and skin-friction coefficient ( $C_f=2\tau_w/\rho_b U_b^2$ ) for heated flow. Here,  $\tau_w$  is the wall shear stress,  $\rho$  is the density and  $U$  is the velocity; subscript 'b' represents the bulk variables. To illustrate these variations, 60 data points were used and the first data point is at  $z=0.195xD$ . A common observation is that the peak in wall temperature increases with increase in the heat flux, indicating the intense heat transfer deterioration. With the increase in the heat flux, the variations of properties will increase and it negatively affects the heat transfer to sCO<sub>2</sub>. This is attributed by the buoyancy and acceleration [8,10,12]. Also, one can compare from fig. 3 that heat transfer deterioration is delayed with the decrease in the inlet temperature, which is obvious due to the far away from the non-linear properties variation region. In most of the cases, heat transfer recovery can be seen after the deterioration. We found that this recovery is brought by the inward and wall-normal motions instead of sweep and ejection events of turbulent shear stress generation. With the increase in the pipe diameter, skin friction rises drastically (see Fig. 4e). The local peak of it reduces by a factor of 2.5 when the inlet temperature is much lower than the pseudocritical temperature. With the increase in pipe diameter and heat flux, friction loss increases due to buoyancy effects increase and it contributes positively to skin friction.



**Figure 5: Variation of; (a): wall temperature, (b): skin friction coefficient;  $D= 2$  mm,  $P_0= 8.8$  MPa,  $T_0= 342$  K,  $q= 30.87$  kW/m<sup>2</sup> (Case 43-45); Note: direction is right to left due to the cooling**

Figure 5 shows the variation in wall temperature and wall shear stress for the cooling case in which  $P_0= 8.8$  MPa for all three possibilities in a vertical pipe. The wall temperature is crucially affected by the direction of fluid flow and its deceleration. In forced convection, only fluid deceleration is present, unlike upward flow where buoyancy also favors the heat transfer. Therefore, the trend of wall temperature are similar to case upward flow case, but with a reduced value. While the downward flow case suffers from the heat transfer deterioration in cooling. Further cases are not presented here due to the page limits, but all these 47 cases can be obtained<sup>1</sup>. We have examined the heat transfer deterioration in downward flow during cooling and observed streak stretching in near wall region. This modulation of near-wall turbulence leads to the impaired heat transfer. As soon as streak stretching disappears, turbulence recovers and consequently the heat transfer. It leads to 'M' shape deformation of the mean velocity profile.

**Effect of diameter on skin friction factor:** To quantify the effects of pipe diameter, we use the Fukagata, Iwamoto and Kasagi (FIK) identity [14], which decomposes the skin friction factor into the individual components. Following equation shows this relationship, the operator  $\langle \rangle$  denotes fluctuations based on the cross-sectional area. In this equation,  $C_{f,FIK}$  is the skin friction factor computed by FIK identity using following eq. In the equation,  $C_1$  represents the laminar contribution,  $C_2$  represents the turbulent contribution and  $C_{10}$  represents the buoyancy contribution. Remaining quantities ( $C_3-C_9$ ) are for inhomogeneous contribution due to the variable properties. The quantity with overbar represents the

<sup>1</sup> Available on: <http://www.ike.uni-stuttgart.de/forschung/CO2/DNS/index.en.html>

Reynold averaged, with tilde shows the Favre averaged, with single prime represents the fluctuating part came out due to Reynolds averaging and double prime is the fluctuations based on Favre averaging.

$$\begin{aligned}
C_{f,FIK} = & \underbrace{-\frac{64}{\rho_b U_b^2 D^3} \int_0^R r \bar{\mu} \overline{S_{rz}} r dr}_{C_1} + \underbrace{\frac{64}{\rho_b U_b^2 D^3} \int_0^R r \overline{\rho u_r'' u_z''} r dr}_{C_2} \\
& + \underbrace{\frac{32}{\rho_b U_b^2 D^3} \int_0^R (R^2 - r^2) \left\langle \frac{\partial \bar{p}}{\partial z} \right\rangle r dr}_{C_3} + \underbrace{\frac{64}{\rho_b U_b^2 D^3} \int_0^R r \bar{\rho} \tilde{u}_r \tilde{u}_z r dr}_{C_4} \\
& + \underbrace{\frac{32}{\rho_b U_b^2 D^3} \int_0^R (R^2 - r^2) \left\langle \frac{\partial \bar{\rho} \tilde{u}_z \tilde{u}_z}{\partial z} \right\rangle r dr}_{C_5} + \underbrace{\frac{32}{\rho_b U_b^2 D^3} \int_0^R (R^2 - r^2) \left\langle \frac{\partial \bar{\rho} u_z'' u_z''}{\partial z} \right\rangle r dr}_{C_6} \\
& - \underbrace{\frac{32}{\rho_b U_b^2 D^3} \int_0^R (R^2 - r^2) \left\langle \frac{1}{r} \frac{\partial r \bar{\mu}' S_{rz}'}{\partial r} \right\rangle r dr}_{C_7} - \underbrace{\frac{32}{\rho_b U_b^2 D^3} \int_0^R (R^2 - r^2) \left\langle \frac{\partial \bar{\mu} S_{zz}}{\partial z} \right\rangle r dr}_{C_8} \\
& - \underbrace{\frac{32}{\rho_b U_b^2 D^3} \int_0^R (R^2 - r^2) \left\langle \frac{\partial \bar{\mu}' S_{zz}'}{\partial z} \right\rangle r dr}_{C_9} \pm \underbrace{\frac{32}{\rho_b U_b^2 D^3} \int_0^R g (R^2 - r^2) \langle \bar{\rho} \rangle r dr}_{C_{10}}
\end{aligned}$$

Figure 5 illustrates the implementation of this identity on two of cases with same boundary conditions except the diameter. The variation of  $C_1$ ,  $C_2$ ,  $C_4$ ,  $C_5$ , and  $C_{10}$  can be seen; the remaining parts which are not shown here have negligible magnitude. Figure 5(a) corresponds to the  $D=2$  mm and fig. 5(b) corresponds to  $D=10$  mm. The first observation is that the symbol ( $C_{f,DNS}$ ) and line in cyan ( $C_{f,FIK}$ ) overlaps which suggests that accuracy of identity and its implementation on our cases. We can observe from both the figures that  $C_{10}$  which is buoyancy part have the highest contribution to the skin friction factor. With the larger pipe diameter, the effects of buoyancy are more severe on hydraulics. While the turbulent part ( $C_2$ ) and inhomogeneous part ( $C_4$ - $C_5$ ) equally affects the  $C_f$ .

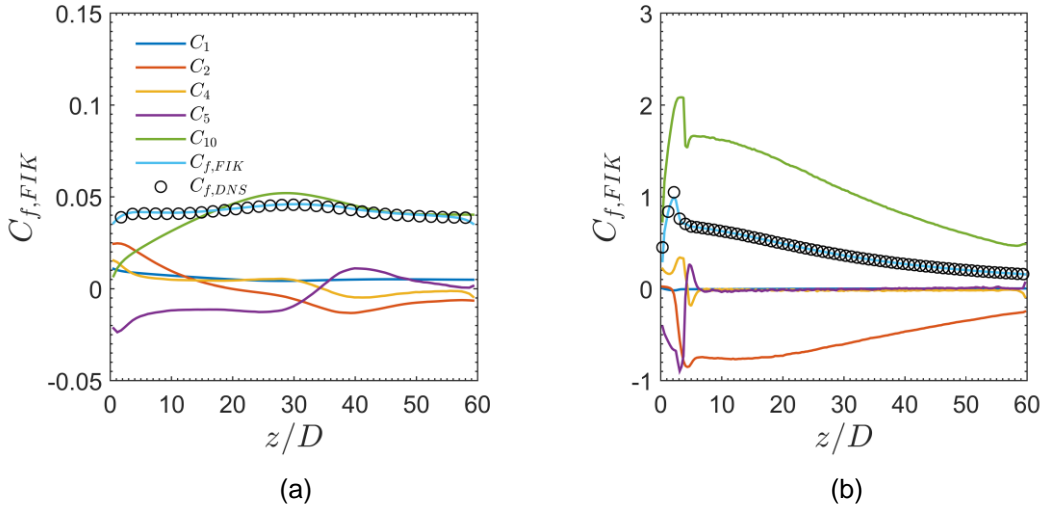


Figure 5: Decomposition of skin friction coefficient for case (a) 2-U(2,8,301,20) (b) 27-U(10,8,301,20)

## SUMMARY

Due to wide applicability of supercritical carbon dioxide, we conducted a series of numerical experiments by using the direct numerical simulation. These simulations have been conducted with positive as well as negative heat flux to resemble the uniform heating and cooling, respectively. The diameter of the tube ranges in between 2 to 10 mm. DNS includes the variation of inlet pressure, pipe diameter, inlet temperature, and heat flux. The characteristics of cooling and heating at supercritical pressure are just opposite to each other for upward and downward flow in a vertical pipe. Heat transfer is deteriorated in

upward heating and downward cooling cases while enhancement occurs in downward heating and upward cooling. With the increase in pipe diameter and heat flux, buoyancy effects increase. This ultimately results in an increase in the skin friction coefficient. Further analysis was conducted using the FIK identity which decomposes the skin friction factor, and it reveals that turbulent contribution decreases in the upward flow. It was also found out that the buoyancy term has a major contribution to the skin friction coefficient and it results in an increased friction with an increase in pipe diameter. This work not only limited to the investigation of heat transfer but with this work, we are delivering a comprehensive DNS database. This database can be used in benchmarking of turbulence models, empirical fitting of the coefficient in correlations and training of machine learning algorithm.

## REFERENCES

1. V. Dostal, M. Driscoll, P. Hejzlar, A supercritical carbon dioxide cycle for next generation nuclear reactors. Tech. rep. MIT (2004).
2. Y. Ahn, S.J. Bae, M. Kim, S.K. Cho, S. Baik, J.I. Lee, J.E. Cha, Review of supercritical CO<sub>2</sub> power cycle technology and current status of research and development, *Nucl. Eng. Technol.* 47 (6) (2015) 647–661.
3. E. Lemmon, M. Huber, M. McLinden, NIST standard reference database 23: reference fluid thermodynamic and transport properties-REFPROP, version 9.1 (2013).
4. H. Kim, Y. Bae, H. Kim, J. Soong, B. Cho, Experimental investigation on the heat transfer characteristics on a vertical upward flow of supercritical CO<sub>2</sub>, in: *Proc. ICAPP, Reno, NV* (2006).
5. S. He, W. Kim, J. Bae, Assessment of performance of turbulence models in predicting supercritical pressure heat transfer in a vertical tube, *Int. J. Heat Mass Transfer* 51 (19–20) (2008) 4659–4675.
6. M. Sharabi, W. Ambrosini, S. He, J. Jackson, Prediction of turbulent convective heat transfer to a fluid at supercritical pressure in square and triangular channels, *Ann. Nucl. Energy* 35 (6) (2008) 993–1005.
7. A. Pucciarelli, I. Borroni, M. Sharabi, W. Ambrosini, Results of 4-equation turbulence models in the prediction of heat transfer to supercritical pressure fluids, *Nucl. Eng. Des.* 281 (2015) 5–14.A.
8. J.H. Bae, J.Y. Yoo, H. Choi, Direct numerical simulation of turbulent supercritical flows with heat transfer, *Phys. Fluids* 17 (10) (2005).
9. X. Chu, E. Laurien, Flow stratification of supercritical CO<sub>2</sub> in a heated horizontal pipe, *J. Supercrit. Fluids* 116 (2016) 172–189.
10. H. Nemati, A. Patel, B.J. Boersma, R. Pecnik, Mean statistics of a heated turbulent pipe flow at supercritical pressure, *Int. J. Heat Mass Transfer* 83 (2015) 741–752.
11. X. Chu, E. Laurien, D.M. McEligot, Direct numerical simulation of strongly heated air flow in a vertical pipe, *Int. J. Heat Mass Transfer* 101 (2016) 1163–1176.
12. X. Chu, E. Laurien, Direct numerical simulation of heated turbulent pipe flow at supercritical pressure, *J. Nucl. Eng. Radiat. Sci.* (2) (2016).
13. S. Pandey, E. Laurien, X. Chu, A modified convective heat transfer model for heated pipe flow of supercritical carbon dioxide, *Int. J. Therm. Sci.* 117 (2017) 227–238.
14. K. Fukagata, K. Iwamoto, and N. Kasagi, Contribution of Reynolds stress distribution to the skin friction in wall-bounded flows," *Physics of Fluids* 14 (2002).

## **ACKNOWLEDGMENTS**

The first author expresses his deep gratitude to the *Forschungsinstitut für Kerntechnik und Energiewandlung (KE) e.V. Stuttgart*, for the doctoral research fellowship. All authors are sincerely thankful to the *High Performance Computing Center (HLRS) Stuttgart* for their support and providing access to the Hazelhen supercomputer.